Weierstraß-Institut

für Angewandte Analysis und Stochastik

Leibniz-Institut im Forschungsverbund Berlin e. V.

Aspects of guaranteed error control in CPDEs

Carsten Carstensen[1] Christian Merdon[1] , Johannes Neumann[2]

submitted: March 25, 2013

[1] Humboldt-Universität zu Berlin
    Unter den Linden 6
    10099 Berlin
    Germany
    email: cc@mathematik.hu-berlin.de
           merdon@mathematik.hu-berlin.de

[2] Weierstraß-Institute
    Mohrenstr. 39
    10117 Berlin
    Germany
    email: Johannes.Neumann@wias-berlin.de

Abstract

Whenever numerical algorithms are employed for a reliable computational forecast, they need to allow for an error control in the final quantity of interest. The discretisation error control is of some particular importance in computational PDEs (CPDEs) where guaranteed upper error bounds (GUB) are of vital relevance. After a quick overview over energy norm error control in second-order elliptic PDEs, this paper focuses on three particular aspects. First, the variational crimes from a nonconforming finite element discretisation and guaranteed error bounds in the discrete norm with improved postprocessing of the GUB. Second, the reliable approximation of the discretisation error on curved boundaries and, finally, the reliable bounds of the error with respect to some goal-functional, namely, the error in the approximation of the directional derivative at a given point.

1   Introduction

A posteriori finite element error control of second-order elliptic boundary value problems usually involves residuals of the proto-type

1

$$\mathrm{Res}(v) = \int_{\Omega} (fv - \sigma_h \cdot \nabla v)\,\mathrm{d}x \quad \text{for } v \in V := H_0^1(\Omega) \tag{1}$$

with some given Lebesgue integrable function f and the discrete flux σ_h [10, 11]. Its dual norm with respect to some energy norm $\|\!|\cdot|\!\|$ reads

$$\|\!|\mathrm{Res}|\!\|_{\star} := \sup_{v \in V} \mathrm{Res}(v) / \|\!|v|\!\|.$$

For instance, the Poisson model problem seeks $u \in V$ with $f + \Delta u = 0$ and leads to the variational formulation

$$\int_{\Omega} \nabla u \cdot \nabla v\,\mathrm{d}x = \int_{\Omega} fv\,\mathrm{d}x \quad \text{for all } v \in V.$$

In this example, the energy norm reads $\|\!|\cdot|\!\| := \|\nabla \cdot\|_{L^2(\Omega)}$ and $\sigma_h = \nabla u_h$ might be the gradient of the piecewise affine conforming finite element solution u_h.

Section 2 summarises techniques and recent advances from the ongoing computational surveys [12, 4, 14] to compute guaranteed upper bounds for $\|\!|\mathrm{Res}|\!\|_{\star}$, or error majorants in the sense of Repin [22], via the design of some $q \in H(\mathrm{div}, \Omega)$ such that, by a triangle inequality,

$$\|\!|\mathrm{Res}|\!\|_{\star} \leqslant \|\!|f + \mathrm{div}\,q|\!\|_{\star} + \|\!|\mathrm{div}(q - \sigma_h)|\!\|_{\star}.$$

While $\|\!|f + \mathrm{div}\,q|\!\|_{\star}$ may lead to oscillations or other higher-order terms, the second term is often estimated suboptimally as $\|\!|\mathrm{div}(q - \sigma_h)|\!\|_{\star} \leqslant \|q - \sigma_h\|_{L^2(\Omega)}$. A new generation of equilibration error estimators is based on

$$\|\!|\mathrm{div}(q - \sigma_h)|\!\|_{\star} = \min_{v \in H^1(\Omega)} \|q - \sigma_h - \mathrm{Curl}\,v\|_{L^2(\Omega)}$$

and the novel postprocessing from [14] improves the efficiency at almost no extra costs. Section 2 reports on the superiority of those error estimates with an application to the conforming P_1 finite element method for the Poisson model problem.

Section 3 examines the nonconforming Crouzeix-Raviart approximations u_{CR} and its discrete flux $\sigma_h = \nabla_{\mathrm{NC}} u_{\mathrm{CR}}$ for the Poisson model problem. The Helmholtz decomposition allows a split of the broken energy error norm into

$$\|u - u_{\mathrm{CR}}\|_{\mathrm{NC}}^2 = \|\!|\mathrm{Res}|\!\|_{\star}^2 + \|\!|\mathrm{Res}_{\mathrm{NC}}|\!\|_{\star}^2.$$

The two residuals Res and $\mathrm{Res}_{\mathrm{NC}}$ allow an estimation via all known a posteriori error estimators. Furthermore, the special structure of the nonconforming residual $\mathrm{Res}_{\mathrm{NC}}$ allows an alternative analysis by the design of conforming companions of u_{CR} [13]. In this paper, we also apply the postprocessed equilibration error estimators to the first residual for even sharper error control beyond [13].

Section 4 extends guaranteed error control to domains with curved boundaries and exemplifies the modifications for some sector domain.

Section 5 establishes guaranteed goal-oriented error estimation where the error $u - u_h$ between the exact and the discrete P_1-FEM solution is *not* measured in the energy norm but with respect to some goal functional $Q \in H^1(\Omega)$. Its Riesz representation solves some dual problem [5, 3] that links the error $Q(e)$ to the energy norms of two perturbed Poisson problems [21]. Lower and upper bounds for those quantities lead to guaranteed bounds for $Q(u - u_h)$.

2 Review of Guaranteed Energy Norm Error Control

This section deals with guaranteed upper bounds for dual norms of residuals by equilibration error estimators. An application to the P_1 conforming finite element method for the Poisson model problem concludes the section.

2.1 Notation

Consider a regular triangulation $\mathscr{T}$ of the simply-connected, polygonal and bounded Lipschitz domain $\Omega \subset \mathbb{R}^2$ into triangles with edges $\mathscr{E}$, nodes $\mathscr{N}$, boundary nodes $\mathscr{N}(\partial\Omega)$ and free nodes $\mathscr{N}(\Omega) := \mathscr{N} \backslash \mathscr{N}(\partial\Omega)$. The midpoints of all edges are denoted by $\mathrm{mid}(\mathscr{E}) := \{\mathrm{mid}(E) \,|\, E \in \mathscr{E}\}$ and the boundary edges along $\partial\Omega$ are denoted by $\mathscr{E}(\partial\Omega) := \{E \in \mathscr{E} \,|\, E \subseteq \partial\Omega\}$ while $\mathscr{E}(\Omega) := \mathscr{E} \backslash \mathscr{E}(\partial\Omega)$ denotes the set of interior edges. The set $\mathscr{T}(E) := \{T \in \mathscr{T} \,|\, E \subset \partial T\}$ contains the neighbouring triangles of the edge $E \in \mathscr{E}$. The open set $\omega_z := \{x \in \Omega \,|\, \varphi_z(x) > 0\}$ for the nodal basis function φ_z is the interior of $\bigcup \mathscr{T}(z)$ for the subtriangulation $\mathscr{T}(z) := \{T \in \mathscr{T} \,|\, z \in \mathscr{N}(T)\}$. The diameter $\mathrm{diam}(T)$ of a triangle T is denoted by h_T. The red-refinement $\mathrm{red}(\mathscr{T})$ of $\mathscr{T}$ is a regular triangulation that refines each triangle $T \in \mathscr{T}$ into four congruent sub-triangles by straight lines through the midpoints of the three edges. With the set $P_k(\mathscr{T})$ of elementwise polynomials of total degree $\leqslant k$, the Raviart-Thomas finite element space of order m reads

$$\mathrm{RT}_m(\mathscr{T}) := \Big\{ q \in H(\mathrm{div}, \Omega) \,\big|\, \forall T \in \mathscr{T} \, \exists a_T, b_T, c_T \in P_m(T)$$
$$\forall x \in T, q(x) = a_T x + (b_T, c_T) \Big\}.$$

The set $C_0(\Omega)$ contains continuous functions with zero boundary conditions along $\partial\Omega$.

2.2 Equilibration Error Estimators

Consider some residual of the form (1) with source function $f \in L^2(\Omega)$ and discrete flux $\sigma_h \in P_0(\mathscr{T};\mathbb{R}^2)$ such that $\mathrm{Res}(\varphi_z) = 0$ for all $z \in \mathscr{N}(\Omega)$. Equilibration error estimators design some quantity $q \in H(\mathrm{div},\Omega)$ such that $\|\!|f + \mathrm{div}\,q\|\!|_\star$ is of higher order and

$$\|\!|\mathrm{Res}\|\!|_\star \leqslant \|\!|f + \mathrm{div}\,q\|\!|_\star + \|\!|\mathrm{div}(\sigma_h - q)\|\!|_\star \,.$$

Two examples for such a design are given through the Braess equilibration error estimator [8, 6] and the Luce-Wohlmuth error estimator [18, 14] which solve at most one-dimensional linear systems of equations around each node $z \in \mathscr{N}$ and design some Raviart-Thomas function $q_B \in \mathrm{RT}_0(\mathscr{T})$ or $q_{LW} \in \mathrm{RT}_0(\mathscr{T}^\star)$ on the dual triangulation $\mathscr{T}^\star$.

The dual mesh $\mathscr{T}^\star$ divides every triangle $T \in \mathscr{T}$ into six subtriangles of same area by connection of the center $\mathrm{mid}(T)$ with the three vertices and the three edge midpoints of T. This results in the two guaranteed upper bounds

$$\eta_B := \|h_\mathscr{T}(f - f_\mathscr{T})\|_{L^2(\Omega)} / j_{1,1} + \|\sigma_h - q_B\|_{L^2(\Omega)} \,, \tag{2}$$

$$\eta_{LW} := \|h_\mathscr{T}(f - f^\star)\|_{L^2(\Omega)} / j_{1,1} + \|\sigma_h - q_{LW}\|_{L^2(\Omega)} \tag{3}$$

for the piecewise integral mean $f_\mathscr{T} \in P_0(\mathscr{T})$, i.e., $f_\mathscr{T}|_T := \fint_T f \, dx$ for $T \in \mathscr{T}$ and $f^\star \in P_0(\mathscr{T}^\star)$ with $f^\star|_{T^\star} := 3 \fint_T f \varphi_z \, dx$ on the two subtriangles $T^\star \in \mathscr{T}^\star(z)$ of $T \in \mathscr{T}(z)$. The function $f^\star$ is our preferred approximation of f in the Luce-Wohlmuth design [14, 16] that allows this very easy estimation of $\|\!|f - f^\star\|\!|_\star$. The number $j_{1,1}$ is the first positive root of the Bessel function J_1 from the Poincaré constant [17].

The definitions (2)-(3) employ the estimate $\|\!|\mathrm{div}(\sigma_h - q)\|\!|_\star \leqslant \|\sigma_h - q\|_{L^2(\Omega)}$, which is suboptimal, because of

$$\|\!|\mathrm{div}(q - \sigma_h)\|\!|_\star = \min_{\gamma \in H^1(\Omega)} \|q - \sigma_h - \mathrm{Curl}\,\gamma\|_{L^2(\Omega)} \,.$$

The novel postprocessing from [14] designs some piecewise affine γ_h that is cheap to compute and leads to sharper estimates. The computation runs some simple pcg scheme with k iterations on a refined triangulation $\mathrm{red}(\mathscr{T})$ or $\mathrm{red}^2(\mathscr{T})$ for η_B and $\mathscr{T}^\star$ for η_{LW}. In the numerical examples below, the number of cg iterations of the postprocessing is added to the label in brackets. Every additional 'r' in front of this number is related to one red-refinement. For example, the error estimator $\eta_{Brr(3)}$ is the postprocessed η_B on two red-refinements with 3 cg iterations. The case $k = \infty$ means an exact solve and leads to the best possible γ; further details on the algorithm are included in [14].

2.3 Poisson Model Problem with Big Oscillations

The Poisson model problem seeks $u \in H_0^1(\Omega)$ with $f + \Delta u = 0$ for some source function $f \in L^2(\Omega)$ on the unit square $\Omega := (0,1)^2$. The conforming FEM seeks $u_h \in V_C := P_1(\mathcal{T}) \cap C_0(\Omega)$ with

$$\int_\Omega \nabla u_h \cdot \nabla v_h \, dx = \int_\Omega f v_h \, dx \quad \text{for all } v_h \in V_C.$$

This leads to the residual (1) with $\sigma_h = \nabla u_h$ and $V_C \subseteq \ker \text{Res}$. Elementary calculations, e.g., in [9], reveal that $\|\text{Res}\|_\star = \|u - u_h\| := \|\nabla(u - u_h)\|_{L^2(\Omega)}$.

The remaining parts of this section concern the benchmark problem with an oscillating source term $f := -\Delta u$ that matches the exact solution

$$u(x,y) = x(x-1)y(y-1)\exp(-100(x-1/2)^2 - 100(y-117/1000)^2) \in H_0^1(\Omega).$$

Figures 1 and 2 show the efficiency indices $\eta_{\text{xyz}}/\|u - u_h\|$ for various GUB η_{xyz} after Braess and Luce-Wohlmuth for uniform and adaptive mesh refinement. The Dörfler marking drives the adaptive mesh-refinement with the refinement indicators

$$\eta(T)^2 := |T| \, \|f\|_{L^2(T)}^2 + |T|^{1/2} \sum_{E \in \mathscr{E}(T)} \|[\sigma_h]_E \cdot \nu_E\|_{L^2(E)}^2. \tag{4}$$

On coarse triangulations, the oscillations dominate the guaranteed upper bounds and the postprocessing is almost effectless. However, as the number of degrees of freedom grows and the oscillations decrease, the efficiency improves and the postprocessing unfolds its full effectivity.

The postprocessing $\eta_{\text{Br}(1)}$ of η_B based on $\text{red}(\mathcal{T})$ and the postprocessing $\eta_{\text{LW}(1)}$ of η_{LW} based on $\mathcal{T}^\star$ reduce the efficiency indices about 20% to values between 1.1 and 1.15, respectively. The optimal postprocessing with $k = \infty$ shows only very little further improvement over the postprocessing with $k = 1$. The postprocessing $\eta_{\text{Brr}(3)}$ of η_B based on two red-refinements $\text{red}^2(\mathcal{T})$ and $k = 3$ iterations even leads to striking efficiency indices of about 1.05.

Similar treatment is possible for conforming obstacle problems [15].

3 Guaranteed Error Control for CR-NCFEM

This section develops sharp guaranteed upper bounds for the broken energy norm

$$\|u - u_{\text{CR}}\|_{\text{NC}}^2 := \sum_{T \in \mathcal{T}} \|\nabla(u - u_{\text{CR}})\|_{L^2(T)}^2$$

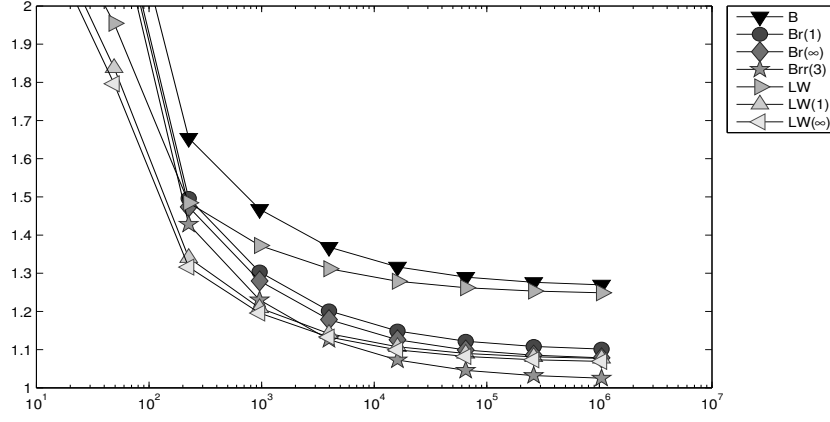for the error between the exact solution u and the Crouzeix-Raviart nonconforming FEM (CR-NCFEM) solution u_{CR}.

Fig. 1 History of efficiency indices $\eta_{xyz}/\|\!|e|\!\|$ of the standard and postprocessed Braess and Luce-Wohlmuth error estimators η_{xyz} labeled *xyz* as functions of ndof on uniform meshes in Subsection 2.3.
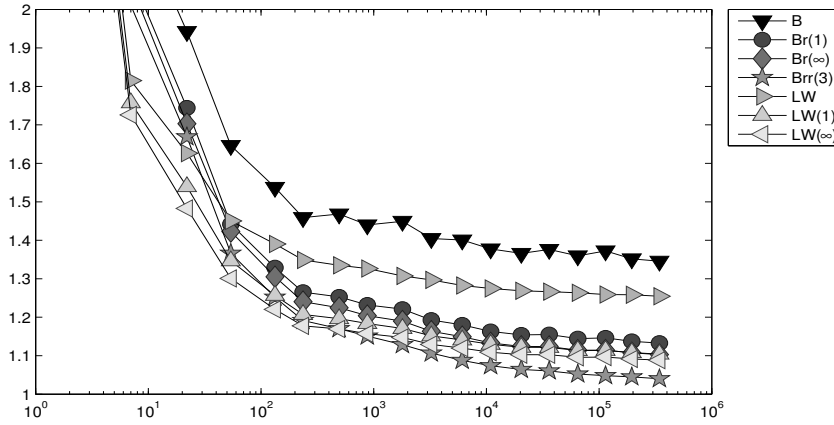

Fig. 2 History of efficiency indices $\eta_{xyz}/\|\!|e|\!\|$ of the standard and postprocessed Braess and Luce-Wohlmuth error estimators η_{xyz} labeled *xyz* in the figure as functions of ndof on adaptive meshes in Subsection 2.3.

3.1 Main Result

The CR-NCFEM employs the Crouzeix-Raviart functions

$$\mathrm{CR}^1(\mathscr{T}) := \{v \in P_1(\mathscr{T}) \,|\, v \text{ is continuous at } \mathrm{mid}(\mathscr{E})\},$$
$$\mathrm{CR}_0^1(\mathscr{T}) := \{v \in \mathrm{CR}^1(\mathscr{T}) \,|\, \forall E \in \mathscr{E}(\partial\Omega), \, v(\mathrm{mid}(E)) = 0\}.$$

The nonconforming finite element approximation $u_{\mathrm{CR}} \in \mathrm{CR}^1_0(\mathscr{T})$ for the Poisson model problem with its piecewise gradient $\nabla_{\mathrm{NC}} u_{\mathrm{CR}}$ satisfies

$$\int_\Omega \nabla_{\mathrm{NC}} u_{\mathrm{CR}} \nabla_{\mathrm{NC}} v_{\mathrm{CR}} dx = \int_\Omega f v_{\mathrm{CR}} \, \mathrm{d}x \quad \text{for all } v_{\mathrm{CR}} \in \mathrm{CR}^1_0(\mathscr{T}).$$

The main result from [13] for the 2D case with a simply-connected domain Ω and homogeneous Dirichlet boundary conditions requires the Helmholtz decomposition of $\nabla_{\mathrm{NC}}(u - u_{\mathrm{CR}}) = \nabla\alpha + \mathrm{curl}\,\beta$ for $\alpha \in H^1_0(\Omega)$ and $\beta \in H^1(\Omega)$. It follows

$$\|u - u_{\mathrm{CR}}\|^2_{\mathrm{NC}} = \||\alpha|\|^2 + \|\mathrm{curl}\,\beta\|^2_{L^2(\Omega)} = \||\mathrm{Res}|\|^2_\star + \||\mathrm{Res}_{\mathrm{NC}}|\|^2_\star$$

with the residuals

$$\mathrm{Res}(v) := \int_\Omega f v \, \mathrm{d}x - \int_\Omega \nabla_{\mathrm{NC}} u_{\mathrm{CR}} \cdot \nabla v \, \mathrm{d}x \qquad \text{for } v \in H^1_0(\Omega),$$

$$\mathrm{Res}_{\mathrm{NC}}(v) := -\int_\Omega \mathrm{curl}_{\mathrm{NC}}\, u_{\mathrm{CR}} \cdot \nabla v \, \mathrm{d}x \qquad \text{for } v \in H^1(\Omega).$$

The dual norm of the second residual allows the alternative characterisation

$$\||\mathrm{Res}_{\mathrm{NC}}|\|_\star = \min_{v \in V} \||u_{\mathrm{CR}} - v|\|_{\mathrm{NC}} \leqslant \||u - u_{\mathrm{CR}}|\|_{\mathrm{NC}}. \tag{5}$$

3.2 Guaranteed Upper Bounds for $\||\mathrm{Res}|\|_\star$

The dual norm of the first residual is controlled [13, 1] by the explicit bound

$$\||\mathrm{Res}|\|^2_\star \leqslant \eta^2 := \sum_{T \in \mathscr{T}} \left(\frac{h_T}{j_{1,1}} \|f - f_\mathscr{T}\|_{L^2(T)} + \frac{f_T}{2} \|\bullet - \mathrm{mid}(T)\|_{L^2(T)} \right)^2. \tag{6}$$

Here, $\mathrm{mid}(T)$ denotes the triangle center of $T \in \mathscr{T}$, and the quantity $\mathrm{osc}(f, \mathscr{T}) := \|h_\mathscr{T}(f - f_\mathscr{T})\|_{L^2(\Omega)}$ denotes the oscillations of f. Since $V_C \subseteq \ker\mathrm{Res}$, $\||\mathrm{Res}|\|_\star$ can also be estimated by any other guaranteed error estimator [10], e.g. the equilibration error estimators from Section 2.

The numerical example from Subsection 2.3 allows for a comparison of the performance of η with that of the Braess and the Luce-Wohlmuth error estimator from Section 2 for the estimation of $\||\mathrm{Res}|\|_\star$. Table 3.2 shows that there is only small improvement of up to 8 percent possible compared to η by $\eta_{\mathrm{LW}(1)}$, the estimator η_{B} is even worse than η. This led to the decision in [13] to employ only η for the estimation of $\||\mathrm{Res}|\|_\star$ in the error control for the nonconforming FEM for the Poisson problem. It seems more favorable to spend effort in the sharp estimation of $\||\mathrm{Res}_{\mathrm{NC}}|\|_\star$.

ndof	8	40	176	736	3008	12160	48896
$\|\|\|u - u_{CR}\|\|\|_{NC}$	0.0583	0.0527	0.0287	0.0198	0.0103	0.00517	0.00259
$osc(f)$	0.223	0.0952	0.0391	0.00938	0.00243	0.000613	0.000154
η	0.233	0.112	0.0521	0.0190	0.00769	0.00336	0.00156
B	0.253	0.140	0.0672	0.0219	0.00835	0.00352	0.00160
LW	0.230	0.116	0.0490	0.0178	0.00737	0.00328	0.00154
Br(1)	0.249	0.133	0.0657	0.0210	0.00796	0.00333	0.00151
Br(∞)	0.248	0.131	0.0654	0.0210	0.00795	0.00333	0.00151
LW(1)	0.229	0.113	0.0477	0.0172	0.00705	0.00312	0.00146
LW(∞)	0.228	0.112	0.0474	0.0172	0.00704	0.00312	0.00146
Brr(3)	0.247	0.128	0.0645	0.0206	0.00782	0.00327	0.00148

Table 1 Guaranteed upper bounds for $\|\|\|Res\|\|\|_\star$ by η and the equilibration error estimators η_B, η_{LW}, and some of their postprocessings for uniform mesh-refinements in the example of Subsection 3.2. The oscillations $osc(f)$ are displayed to show its declining influence to η.

3.3 Guaranteed Upper Bounds for $\|\|\|Res_{NC}\|\|\|_\star$

Since $Res_{NC}(\varphi_z) = 0$ for all $z \in \mathcal{N}$, any equilibration error estimator from Section 2 is applicable (with $\sigma_h = curl\, u_{CR}$ and $f \equiv 0$ in (1)) and leads, e.g., via $q_{xyz} = q_B$ or q_{LW} to the upper bounds

$$\|\|\|Res_{NC}\|\|\|_\star \leqslant \|curl\, u_{CR} - q_{xyz}\|_{L^2(\Omega)} =: \mu_{xyz}.$$

The second characterisation (5) of $\|\|\|Res_{NC}\|\|\|_\star$ allows an upper bound for $\|\|\|Res_{NC}\|\|\|_\star$ by the design of conforming functions $v_{xyz} \in V$ such that

$$\|\|\|Res_{NC}\|\|\|_\star \leqslant \|\|\|u_{CR} - v_{xyz}\|\|\|_{NC} =: \mu_{xyz}.$$

Since $q_{xyz} := curl\, v_{xyz} \in H(div, \Omega)$, those can also be seen as equilibration error estimators and allow the postprocessing of Subsection 2.2. Three designs for some v_{xyz} from [13, 1] are repeated in the sequel.

Ainsworth [1] designs some piecewise linear $v_A \in P_1(\mathcal{T}) \cap C_0(\Omega)$ by averaging on node patches $\mathcal{T}(z) := \{T \in \mathcal{T} \mid z \in T\}$,

$$v_A(z) := \begin{cases} 0 & \text{if } z \in \mathcal{N} \setminus \mathcal{N}(\Omega), \\ \left(\sum_{T \in \mathcal{T}(z)} u_{CR}|_T(z)\right) / |\mathcal{T}(z)| & \text{if } z \in \mathcal{N}(\Omega). \end{cases}$$

The averaging of the auxiliary function from [23, 2, 7]

$$v^0 := u_{CR} - f_{\mathcal{T}}\, \psi / 2 \in P_2(\mathcal{T}),$$

where $\psi(x) := |x - mid(T)|^2 / 2 - f_T |y - mid(T)|^2\, dy$ for $x \in T \in \mathcal{T}$, leads to $v_{AP2} \in P_2(\mathcal{T}) \cap C_0(\Omega)$ via

$$v_{\text{AP2}}(z) := \begin{cases} 0 & \text{if } z \in \mathcal{N}(\partial\Omega) \cup \text{mid}(\mathcal{E}(\partial\Omega)), \\ \left(\sum_{T \in \mathcal{T}(z)} v^0|_T(z)\right)/|\mathcal{T}(z)| & \text{if } z \in \mathcal{N}(\Omega), \\ \left(\sum_{T \in \mathcal{T}(E)} v^0|_T(z)\right)/|\mathcal{T}(E)| & \text{if } z = \text{mid}(E), E \in \mathcal{E}(\Omega). \end{cases}$$

The novel design from [13] employs the red-refined triangulation and defines $v_{\text{RED}}(z) \in P_1(\text{red}(\mathcal{T})) \cap C_0(\Omega)$ via

$$v_{\text{RED}}(z) := \begin{cases} u_{\text{CR}}(z) & \text{for } z \in \text{mid}(\mathcal{E}(\Omega)), \\ 0 & \text{for } z \in \mathcal{N}(\partial\Omega) \cup \text{mid}(\mathcal{E}(\partial\Omega)), \\ v_z & \text{for } z \in \mathcal{N}(\Omega). \end{cases}$$

The values v_z for $z \in \mathcal{N}(\Omega)$ may be chosen by an averaging as above or by patch-wise minimisation as in [13]; this leads to the two averagings v_{ARED} and v_{PMRED}.

3.4 Numerical Experiment with Big Oscillations

This section concludes with the revisit of the example of Subsection 2.3 for the CR-NCFEM. Figures 3 and 4 display the efficiency indices $\eta_{\text{xyz}}/\|e\|$ for all error estimators of Subsection 3.3. Under the label B and LW, both residuals were estimated with the same error estimator, i.e., $\|u - u_{\text{CR}}\|_{\text{NC}}$ is bound by $\eta_B + \mu_B$ and $\eta_{\text{LW}} + \mu_{\text{LW}}$, respectively. The error estimators based on conforming interpolations $\text{xyz} \in \{A, \text{AP2}, \text{ARED}, \text{PMRED}\}$, involve $\|\text{Res}\|_\star \leqslant \eta$ and hence bound $\|u - u_{\text{CR}}\|_{\text{NC}}$ by $\eta + \mu_{\text{xyz}}$. The same holds for their postprocessings. Notice, that r(3) applied to ARED or PMRED means altogether two red-refinements.

The energy error is estimated very effectively with efficiency indices between 1.5 for unpostprocessed estimators like η_B and η_A and about 1.05 for the postprocessed estimators $\eta_{\text{Brr}(3)}$ or $\eta_{\text{Arr}(3)}$.

4 Guaranteed Error Control for Curved Boundaries

Particular attention requires the inexact approximation of the geometry by the polygonal boundary of a triangulation into triangles. This section is devoted to an example for a convex boundary where there is no real need of curved finite elements. The benchmark problem on the sector domain

$$\Omega = \left\{ x = (r\cos\varphi, r\sin\varphi) \,\middle|\, 0 < \varphi < 3\pi/2,\ 0 < r < 1 \right\}$$

from [1] employs the exact solution $u(r, \varphi) = (r^{2/3} - r^2)\sin(2\varphi/3)$ with a typical corner singularity at the reentrant corner.
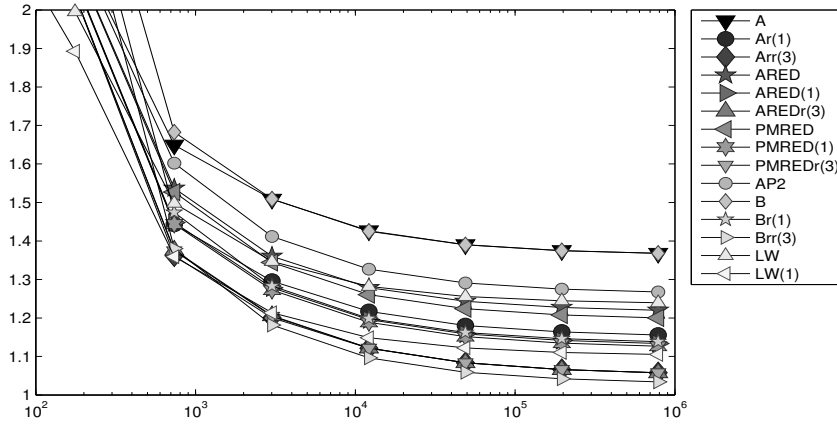
Fig. 3 History of efficiency indices $\eta_{xyz}/\|e\|$ of various error estimators η_{xyz} labeled *xyz* as functions of ndof on uniform meshes in Subsection 3.
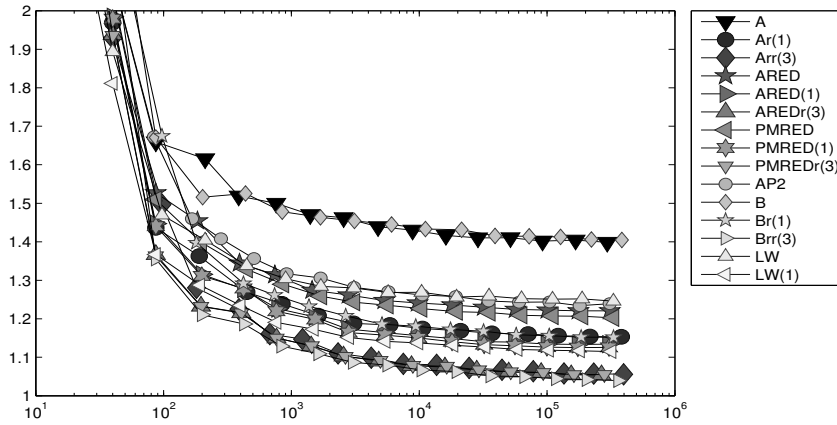

Fig. 4 History of efficiency indices $\eta_{xyz}/\|e\|$ of various error estimators η_{xyz} labeled *xyz* in the figure as functions of ndof on adaptive meshes in Subsection 3.

Since the domain is not matched exactly, $\bigcup \mathscr{T} \subset \overline{\Omega}$ requires extra considerations for u_h extended by zero outside of $\bigcup \mathscr{T}$ such that $u_h \in H_0^1(\Omega)$. The reflection of boundary triangles of Figure 5 yields an extended triangulation $\widehat{\mathscr{T}}$ with $\Omega \subset \bigcup \widehat{\mathscr{T}}$ where the extended source-function $f(\varphi) = 32\sin(2\varphi/3)/9$ is well defined. The new triangles involve only Dirichlet nodes and allow the Braess or Luce-Wohlmuth design of an equilibration q_B or q_{LW} from Section 2.2 on the extended triangulation, possibly with a postprocessing $\gamma_h \in H^1(\bigcup \widehat{\mathscr{T}})$. This results in
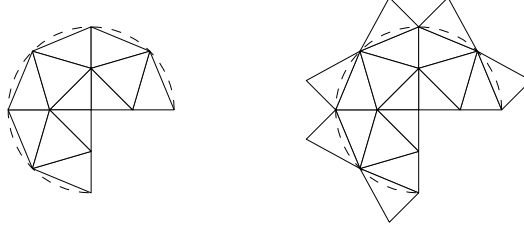
Fig. 5 Triangulation $\mathscr{T}$ (left, solid lines) and extended triangulation $\widehat{\mathscr{T}}$ (right, solid lines) with $\bigcup \mathscr{T} \subseteq \Omega \subseteq \bigcup \widehat{\mathscr{T}}$ for the sector domain Ω (dashed lines) from Section 4.

$$\|\mathrm{Res}\|_{\star} \leqslant \left\| h_{\widehat{\mathscr{T}}}(f + \mathrm{div}\,\widehat{q}) \right\|_{L^2(\bigcup \widehat{\mathscr{T}})} / j_{1,1} + \|\widehat{q} - \sigma_h - \mathrm{Curl}\,\gamma_h\|_{L^2(\Omega)}.$$

The integration of $\widehat{q} - \sigma_h - \mathrm{Curl}\,\gamma_h$ over the non-polygonal domain Ω separates into an exact integration over triangles in $\mathscr{T}$ and an integration over intersections $T \cap \Omega$ of triangles $T \in \widehat{\mathscr{T}} \setminus \mathscr{T}$. The latter integration employs polar coordinates and Gauss quadrature with at least 100 quadrature points.
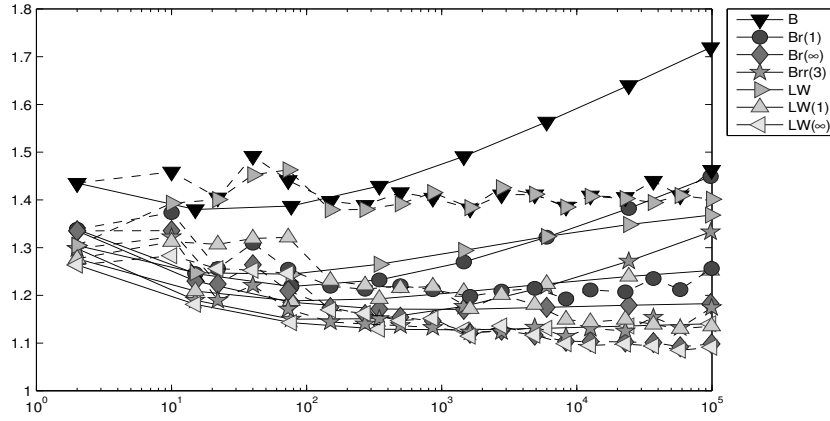

Fig. 6 History of efficiency indices $\eta_{\mathrm{xyz}}/\|e\|$ of the standard and postprocessed Braess and Luce-Wohlmuth error estimators η_{xyz} labeled *xyz* in the figure as functions of the number of unknowns on uniform (solid lines) and adaptive (dashed lines) meshes for the sector example of Section 4.

To consider also the domain approximation error in the adaptive refinement, the refinement indicators (4) are replaced by

$$\eta(T)^2 + 2\,\mathrm{width}(\widehat{T} \cap \Omega)/\pi \, \|f\|_{L^2(\widehat{T} \cap \Omega)} \quad \text{for } T \in \mathscr{T} \text{ with a reflection } \widehat{T} \in \widehat{\mathscr{T}} \setminus \mathscr{T}.$$

Additionally, modified refinement routines shift the midpoints of all bisected edges along the curved boundary onto the unit circle. For simplicity, the postprocessing of Section 2.2 is only applied to vertices $z \in \mathcal{N}$ with $\widehat{\omega}_z \subseteq \Omega$ where $\widehat{\omega}_z$ is the patch with respect to the extended triangulation $\widehat{\mathcal{T}}$. Undocumented experiments show to us that otherwise the efficiency becomes worse.

The oscillations in this example are not as large as in the square example from Subsection 2.3, but the conclusions appear similar. Figure 6 displays the efficiency indices of the two error estimators η_{LW} and η_B. The postprocessed equilibration error estimator $\eta_{LW(1)}$ or $\eta_{Brr(3)}$ permits efficiency indices around 1.2 while $\eta_{Br(1)}$ leads to 1.3 for adaptive mesh refinement. Due to the simple extension of the solution from $\mathcal{T}$ to $\widehat{\mathcal{T}}$, there is a large refinement along the circular boundary edges, but the efficiency is almost as good as in the other examples. As a result, even for curved boundaries, reliable error control is possible and accurate.

For the nonconforming solution u_{CR} a similar treatment is possible, cf. [13] for details.

5 Guaranteed Goal-Oriented Error Estimation

This section is devoted to guaranteed error control with respect to some functional like the derivative $-\partial/\partial x_1 \delta_{x_0}$ evaluated at a point $x_0 = (\pi/7, 49/100)$. Subsection 5.1 describes a way to recast that problem into a computable term plus a linear and bounded goal functional $Q \in H^{-1}(\Omega)$ which in Subsection 5.2 is controlled via the parallelogram identity in terms of energy error estimates. Figure 7 displays the numerical results for a benchmark with an overestimation by a guaranteed bound by just one order of magnitude.

5.1 Reduction to L^2 Functionals

Given some fixed point x_0 in the domain $\Omega = (0,1)^2$, this section aims at guaranteed error bounds of the x_1 derivative $\partial u(x_0)/\partial x_1$. This point value $-\partial \delta_{x_0}/\partial x_1$ is not well-defined for any Sobolev function. This subsection discusses a split of

$$\partial \delta u(x_0)/\partial x_1 = Q(u) + M(f)$$

in a bounded functional $Q(u)$ and an unbounded functional $M(f)$ independent of u [19] that can be computed beforehand. The fundamental solution of the Laplace operator Δ in 2D is $\log r/2\pi$ in polar coordinates (r, ϕ) at x_0, in symbolic notation $2\pi \partial \delta_{x_0} = \Delta \log r$. The derivative $-2\pi \partial \delta_{x_0}/\partial x_1 = \Delta \cos \phi/r$ leads to the formula (recall $x = x_0 + r(\cos \phi, \sin \phi)$)

$$2\pi \frac{\partial v(x_0)}{\partial x_1} = \int_{\Omega} (\cos\phi/r)\Delta v(x)\,\mathrm{d}x \quad \text{for all } v \in \mathscr{D}(\Omega). \tag{7}$$

This identity is the clue to cast the point derivative of the solution of the Laplace equation as a function of the right-hand side $f \in L^2(\Omega) \cap L^p(U)$ for some neighbourhood U of x_0 and some $p > 2$. By local elliptic regularity, u is C^1 in a neighbourhood of x_0 and $\Delta v = -f$ allows for $f/r \in L^1(U)$. Hence, the formula (7) makes sense for the exact solution u. The boundary conditions, however, do not allow to utilize the formula directly for $v = u$ in (7) and so involves some cut-off function χ, which is identically one in some neighbourhood of x_0 and vanishes outside U.

In the example of this section, the spline function η of order 6 on the interval $(0.1, 0.45)$ with natural boundary conditions has been evaluated with MATLAB by

```
spapi(6,[0.1*ones(1,5),0.275,0.45*ones(1,5)],[zeros(1,5),1,zeros(1,5)])
```

to define

$$1 - \chi(r,\phi) := \frac{\int_0^r \eta(s)\,\mathrm{d}s}{\int_0^1 \eta(s)\,\mathrm{d}s} \quad \text{for } 0 < r < 1.$$

With $v := \chi u$ in (7), $\Delta u = f$ in some neighbourhood of x_0 where $r = 0$ is some singularity in the volume integral. The product rule $\Delta v = \chi f + 2\nabla\chi \cdot \nabla u + u\Delta\chi$ shows that

$$\frac{\partial u(x_0)}{\partial x_1} = \int_{\Omega} \frac{\cos\phi}{2\pi r} \chi(x) f(x)\,\mathrm{d}x + Q(u). \tag{8}$$

The point is that the linear functional $Q(u)$ involves smooth functions like $\nabla\chi/r$ (which vanishes near x_0) as well as u and its derivative ∇u and hence is linear, bounded and $Q \in H^{-1}(\Omega)$. Indeed, some further integration by parts reveals that

$$Q(u) = \int_{\Omega} g(x) u(x)\,\mathrm{d}x \quad \text{for } g(x) := -\nabla\chi(x) \cdot \nabla\left(\frac{\cos\phi}{\pi r}\right) - \frac{\cos\phi}{2\pi r}\Delta\chi. \tag{9}$$

Recall that $\chi \equiv 1$ in a neighbourhood of $r = 0$ and so $g \in L^2(\Omega)$ is smooth. Since the first integral on the right-hand side of (8) is known and computable, the computation of the unbounded functional $-\partial\delta_{x_0}/\partial x_1$ is reduced to that of the bounded functional Q of the following subsection.

5.2 Guaranteed Bounds for Goal Functionals

Given some L^2 function g and the goal-functional Q from (9) the estimation of $Q(u - u_h)$ is driven by $g \in L^2(\Omega)$ as the right-hand side, the exact solution z and the discrete solution z_h of the adjoint problem [5, 3]. Then, the parallelogram identity for any $\alpha \neq 0$ yields

$$Q(u - u_h) = \frac{1}{4} \left\| \alpha(u - u_h) + \frac{z - z_h}{\alpha} \right\|^2 - \frac{1}{4} \left\| \alpha(u - u_h) - \frac{z - z_h}{\alpha} \right\|^2. \qquad (10)$$

As in [21], upper and lower bounds for the energy norm terms imply corresponding bounds for the error $Q(u - u_h)$. Note, that lower bounds can be designed from upper bounds and vice versa with the hyper circle identity

$$\|p - p_{\mathrm{RT}}\|_{L^2(\Omega)}^2 + \|p - \nabla u_h\|_{L^2(\Omega)}^2 = \|p_{\mathrm{RT}} - \nabla u_h\|_{L^2(\Omega)}^2 + 2(u - u_h, f - f_{\mathscr{T}})$$

for the Raviart-Thomas solution $p_{\mathrm{RT}} \in \mathrm{RT}_0(\mathscr{T})$ [20, 6]. The upper bound

$$\|p - p_{\mathrm{RT}}\|_{L^2(\Omega)}^2 \leqslant \frac{\mathrm{osc}^2(f, \mathscr{T})}{j_{1,1}^2} + \mathrm{dist}^2(p_{\mathrm{RT}}, \nabla H_0^1(\Omega))$$

employs the Helmholtz decomposition $p - p_{\mathrm{RT}} = \nabla \alpha + \mathrm{Curl}\,\beta$ with $\nabla \alpha \perp \mathrm{Curl}\,\beta$ and the Poincaré constant from Subsection 2.2. Any $v \in H_0^1(\Omega)$ satisfies

$$\begin{aligned}
\|p - p_{\mathrm{RT}}\|_{L^2(\Omega)}^2 &= \|\alpha\|^2 + \|\beta\|^2 = (\nabla \alpha, p - p_{\mathrm{RT}}) + (\mathrm{Curl}\,\beta, p - p_{\mathrm{RT}}) \\
&= -(\alpha, \mathrm{div}\,p - \mathrm{div}\,p_{\mathrm{RT}}) + (\mathrm{Curl}\,\beta, \nabla v - p_{\mathrm{RT}}) \\
&= (\alpha - \alpha_{\mathscr{T}}, f - f_{\mathscr{T}}) + (\mathrm{Curl}\,\beta, \nabla v - p_{\mathrm{RT}}) \\
&\leqslant \|\alpha\| \frac{\mathrm{osc}(f, \mathscr{T})}{j_{1,1}} + \|\beta\| \, \mathrm{dist}(p_{\mathrm{RT}}, \nabla H_0^1(\Omega)) \\
&\leqslant \left(\frac{\mathrm{osc}^2(f, \mathscr{T})}{j_{1,1}} + \mathrm{dist}^2(p_{\mathrm{RT}}, \nabla H_0^1(\Omega)) \right)^{1/2} \left(\|\alpha\|^2 + \|\beta\|^2 \right)^{1/2}.
\end{aligned}$$

The upper bound $\|u - u_h\| \leqslant \mathrm{osc}(f, \mathscr{T})/j_{1,1} + \|u_M - u_h\|$ incorporates a function u_M similar to v^0 from Subsection 3.3, but here u_{CR} is the *CR* solution for the right-hand side $f_{\mathscr{T}}$ to ensure $\nabla_{NC} u_M = p_{\mathrm{RT}}$ [23]. This leads to

$$\begin{aligned}
\|u - u_h\| &= \sup_{\|v\|=1} (F(v) - a(u_h, v)) = \sup_{\|v\|=1} ((f - \mathrm{div}\,p_{\mathrm{RT}}, v) + (p_{\mathrm{RT}} - \nabla u_h, \nabla v)) \\
&\leqslant \frac{\mathrm{osc}(f, \mathscr{T})}{j_{1,1}} + \sup_{\|v\|=1} (\nabla v, \nabla_{NC} u_M - \nabla u_h).
\end{aligned}$$

With the convention scheme $u^+ = \alpha u + z/\alpha$, $u^- = \alpha u - z/\alpha$, $f^+ = \alpha f + g/\alpha$ and $f^- = \alpha f - g/\alpha$ those bounds imply guaranteed upper and lower bounds for (10). As in Subsection 3.3, an averaging of u_M results in a continuous $P_2(\mathscr{T})$ function u_A which gives an upper bound for $\mathrm{dist}(p_{\mathrm{RT}}, \nabla H_0^1(\Omega))$. Altogether, this leads to guaranteed upper and lower bounds for $Q(u - u_h)$,

$$\eta_A^+ = \frac{1}{4}\left(\left(\frac{\mathrm{osc}(f^+,\mathscr{T})}{j_{1,1}} + \left\|\!\left\|u_M^+ - u_h^+\right\|\!\right\|\right)^2 - \left\|p_{\mathrm{RT}}^- - \nabla u_h^-\right\|_{L^2(\Omega)}^2 + \frac{3\,\mathrm{osc}^2(f^-,\mathscr{T})}{2j_{1,1}^2}\right.$$

$$\left. + \left\|p_{\mathrm{RT}}^- - \nabla u_A\right\|_{L^2(\Omega)} + 2\left\|\!\left\|u_M^- - u_h^-\right\|\!\right\|\frac{\mathrm{osc}(f^-,\mathscr{T})}{j_{1,1}}\right),$$

$$\eta_A^- = \frac{1}{4}\left(\left\|p_{\mathrm{RT}}^+ - \nabla u_h^+\right\|_{L^2(\Omega)}^2 - \frac{3\,\mathrm{osc}^2(f^+,\mathscr{T})}{2j_{1,1}^2} - \left\|p_{\mathrm{RT}}^+ - \nabla u_A\right\|_{L^2(\Omega)}\right.$$

$$\left. - 2\left\|\!\left\|u_M^+ - u_h^+\right\|\!\right\|\frac{\mathrm{osc}(f^+,\mathscr{T})}{j_{1,1}} - \left(\frac{\mathrm{osc}(f^-,\mathscr{T})}{j_{1,1}} + \left\|\!\left\|u_M^- - u_h^-\right\|\!\right\|\right)^2\right).$$

Elementary calculations show that $\alpha_A := (\|\!\|z_M - z_h\|\!\| / \|\!\|u_M - u_h\|\!\|)^{1/2}$ is the optimal choice for the parameter α. The same bounds yield an upper bound η_C for the Cauchy inequality $|Q(u - u_h)| \leqslant \|\!\|u - u_h\|\!\|\,\|\!\|z - z_h\|\!\| \leqslant \eta_C$.

5.3 Benchmark Example

The function $f = 2x - 2x^2 + 2y - 2y^2$ with the analytical solution $u = x(1-x)y(1-y)$ and the reduction from Subsection 5.1 leads to some smooth known function g. Standard quadrature resolves the unbounded functional and adaptive goal oriented FEM handles the bounded functional Q. The adaptive mesh-refinement algorithm employs the refinement rules from [19]. They employ Dörfler marking separately for the primal and the dual problem and choose the smaller set of marked edges for the final mesh refinement.

Figure 7 displays the error $|Q(u - u_h)|$, η_C, the guaranteed error bound $\left|\eta_A^+ - \eta_A^-\right|$ /2 for $\left|Q(u - u_h) - (\eta_A^+ + \eta_A^-)/2\right|$ and the L^2 norm of the error $u - u_h$ in the primal problem. The a posteriori error control of the L^2 error $\|u - u_h\|_{L^2(\Omega)}$ in the primal problem is possible in this example on a convex domain but significantly harder for nonconvex polygons. In the general case, the duality argument requires the precise values for the reduced elliptic regularity to deduce guaranteed error bounds.
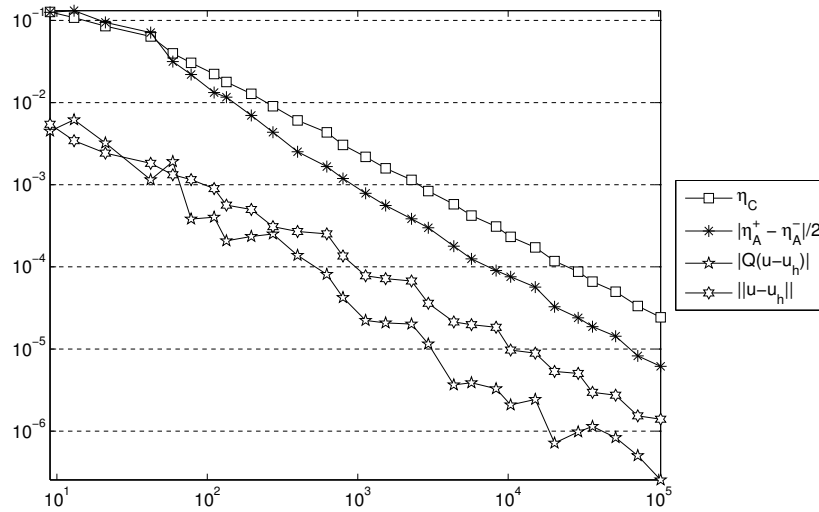
Acknowledgements

Fig. 7 Convergence history of the error $|Q(u - u_h)|$, $\left|\eta_A^+ - \eta_A^-\right|/2$, η_C and $\|u - u_h\|_{L^2(\Omega)}$.

References

1. Mark Ainsworth. Robust a posteriori error estimation for nonconforming finite element approximation. *SIAM J. Numer. Anal.*, 42(6):2320–2341, 2004.
2. Mark Ainsworth. A posteriori error estimation for lowest order Raviart-Thomas mixed finite elements. *SIAM J. Sci. Comput.*, 30(1):189–204, 2007/08.
3. Wolfgang Bangerth and Rolf Rannacher. *Adaptive finite element methods for differential equations*. Lectures in Mathematics ETH Zürich. Birkhäuser Verlag, Basel, 2003.
4. S. Bartels, C. Carstensen, and R. Klose. An experimental survey of a posteriori Courant finite element error control for the Poisson equation. *Adv. Comput. Math.*, 15(1-4):79–106, 2001.
5. Roland Becker and Rolf Rannacher. An optimal control approach to a posteriori error estimation in finite element methods. *Acta Numer.*, 10:1–102, 2001.
6. Dietrich Braess. *Finite elements*. Cambridge University Press, Cambridge, third edition, 2007. Theory, fast solvers, and applications in elasticity theory.
7. Dietrich Braess. An a posteriori error estimate and a comparison theorem for the nonconforming P_1 element. *Calcolo*, 46(2):149–155, 2009.
8. Dietrich Braess and Joachim Schöberl. Equilibrated residual error estimator for edge elements. *Math. Comp.*, 77(262):651–672, 2008.
9. S.C. Brenner and C. Carstensen. *Finite Element Methods, Encyclopedia of Computational Mechanics (Chapter 4)*. John Wiley and Sons, 2004.
10. C. Carstensen. A unifying theory of a posteriori finite element error control. *Numer. Math.*, 100(4):617–637, 2005.
11. C. Carstensen, M. Eigel, R. H. W. Hoppe, and C. Loebhard. Numerical mathematics: Theory, methods and applications. *Numer. Math. Theor. Meth. Appl.*, 5(4):509–558, 2012.
12. Carsten Carstensen and Christian Merdon. Estimator competition for Poisson problems. *J. Comp. Math.*, 28(3):309–330 (electronic), 2010.
13. Carsten Carstensen and Christian Merdon. Computational survey on a posteriori error estimators for nonconforming finite element methods for Poisson problems (submitted). *Preprint available under http://www2.mathematik.hu-berlin.de/publ/pre/2012/P-12-12.pdf*, 2012+.

14. Carsten Carstensen and Christian Merdon. Effective postprocessing for equilibration a posteriori error estimators. *Numer. Math*, 2012.
15. Carsten Carstensen and Christian Merdon. A posteriori error estimator competition for conforming obstacle problems. *Numer. Methods Partial Differential Eq., Preprint available under http://www2.mathematik.hu-berlin.de/publ/pre/2012/P-12-01.pdf*, 2012.
16. Carsten Carstensen and Christian Merdon. Refined fully explicit a posteriori residual-based error control (submitted). 2012+.
17. R. S. Laugesen and B. A. Siudeja. Minimizing Neumann fundamental tones of triangles: an optimal Poincaré inequality. *J. Differential Equations*, 249(1):118–135, 2010.
18. R. Luce and B. I. Wohlmuth. A local a posteriori error estimator based on equilibrated fluxes. *SIAM J. Numer. Anal.*, 42(4):1394–1414, 2004.
19. M. S. Mommer and R. Stevenson. A goal-oriented adaptive finite element method with convergence rates. *SIAM Journal on Numerical Analysis*, 47(2):861–886, 2009.
20. W. Prager and J. L. Synge. Approximations in elasticity based on the concept of function space. *Quart. Appl. Math.*, 5:241–269, 1947.
21. S. Prudhomme and J. T. Oden. On goal-oriented error estimation for elliptic problems: application to the control of pointwise errors. *Comput. Methods Appl. Mech. Engrg.*, 176(1-4):313–331, 1999. New advances in computational methods (Cachan, 1997).
22. S. Repin. *A Posteriori Estimates for Partial Differential Equations*, volume 4 of *Radon Series on Computational and Applied Mathematics*. Walter de Gruyter, Berlin, 2008.
23. Martin Vohralík. A posteriori error estimates for lowest-order mixed finite element discretizations of convection-diffusion-reaction equations. *SIAM J. Numer. Anal.*, 45(4):1570–1599, 2007.